Electronic Supplementary Information

Experimental Section

Materials: Sodium hydroxide (NaOH), ammonium chloride (NH_4Cl), salicylic acid ($C_7H_6O_3$), sodium citrate dehydrate ($C_6H_5Na_3O_7·2H_2O$), *p*-dimethylaminobenzaldehyde ($C_9H_{11}NO$), sodium nitroferricyanide dihydrate ($C_5FeN_6Na_2O·2H_2O$), sodium dihydrogen phosphate dihydrate ($NaH_2PO_4·2H_2O$), disodium hydrogen phosphate dodecahydrate ($Na_2HPO_4·12H_2O$), sodium nitrate ($NaNO_3$) and sodium hypochlorite (NaClO), were purchased from Aladdin Ltd. (Shanghai, China). Sulfuric acid (H_2SO_4), hydrogen peroxide (H_2O_2), hydrochloric acid (HCl), hydrazine monohydrate ($N_2H_4·H_2O$), phosphoric acid (H_3PO_4) and ethylalcohol (C_2H_5OH) were purchased from Beijing Chemical Corporation. (China). chemical Ltd. in Chengdu. Cobalt nitrate ($Co(NO_3)_2·6H_2O$), melamine ($C_3H_6N_6$), were purchased from Chengdu Kelong Chemical Regent Co. Ltd. Carbon paper (CP) was purchased from Qingyuan Metal Materials Co., Ltd (Xingtai, China). All reagents used in this work were analytical grade without further purification. The ultrapure water purified on a Millipore system was used in all experiments.

Synthesis of Co-NCNT and pure Co particle: Co-NCNT nanohybrid was prepared as follows: Firstly, 0.291 g $Co(NO_3)_2·6H_2O$, 2.102 g melamine, a certain amount of ethylalcohol were mixed and ground in a mortar for 30 min. Then the mixture was dried at 60 °C. After that, it was placed in a tube furnace with pyrolysis treatment at 800 °C for 2 h under H_2/Ar atmosphere. Finally, the Co-NCNT nanohybrid can be obtained. As a control, the pure Co particle was prepared by the same fabrication process of Co-NCNT but without melamine.

Characterizations: XRD data were acquired by a LabX XRD-6100 X-ray diffractometer with a Cu Kα radiation (40 kV, 30 mA) of wavelength 0.154 nm (SHIMADZU, Japan). SEM measurements were carried out on a Gemini SEM 300 scanning electron microscope (ZEISS, Germany) at an accelerating voltage of 5 kV.

TEM image was obtained from a Zeiss Libra 200FE transmission electron microscope operated at 200 kV. XPS measurements were performed on an ESCALABMK II X-ray photoelectron spectrometer using Mg as the exciting source. The absorbance data was measured on on SHIMADZU UV-1800 Ultraviolet-visible (UV-Vis) spectrophotometer. Gaseous products from nitrate reduction reaction were determined by GC with SHIMADZU GC-2014 gas chromatograph. A GC run was initiated per 1200 s. Argon (99.999%) was used as the carrier gas. A flame ionization detector with a thermal conductivity detector (TCD) was used to quantify hydrogen and nitrogen. The electrolyzer outlet was introduced into a condenser before being vented directly into the gas sampling loop of the gas chromatograph.

Electrochemical measurements: All electrochemical measurements were carried on the CHI660E electrochemical workstation (Shanghai, Chenhua) using a standard three-electrode setup. Electrolyte solution was Ar-saturated of 0.1 M NaOH with 0.1 M NO_3^-, using Co-NCNT or Co particle (loading 0.5 mg) on CP as working electrode (identified as Co-NCNT/CP or Co/CP), a graphite rod as the counter electrode, and a Hg/HgO as the reference electrode. We use a H-type electrolytic cell separated by a Nafion 117 membrane which was protonated by boiling in ultrapure water, H_2O_2 (5%) aqueous solution and 0.5 M H_2SO_4 at 80 °C for another 2 h, respectively. All the potentials reported in our work were converted to reversible hydrogen electrode via calibration with the following equation: E (RHE) = E (Hg/HgO) + (0.098 + 0.0591 × pH) V and the presented current density was normalized to the geometric surface area.

Determination of NH_3: The NH_3 concentration in the solution was determined by colorimetry (the obtained electrolyte was diluted 40 times) using the indophenol blue method.[1] In detail, 2 mL of the solution after reaction, and 2 mL of 1 M NaOH coloring solution containing 5% salicylic acid and 5% sodium citrate. Then, 1 mL oxidizing solution of 0.05 M NaClO and 0.2 mL catalyst solution of $C_5FeN_6Na_2O$ (1 wt%) were added to the above solution. After standing in the dark for 2 h, the UV-Vis absorption spectra were measured. The concentration of NH_3 was identified using the

absorbance at a wavelength of 655 nm. The concentration-absorbance curve was calibrated using the standard NH_4Cl solution with NH_3 concentrations of 0, 0.2, 0.5, 1.0, 2.0, and 5.0 ppm in 0.1 M NaOH solution. The fitting curve (y = 0.39320x + 0.03725, R^2 = 0.9999) shows good linear relation of absorbance value with NH_3 concentration.

Detection of NO_2^-: The concentration of NO_2^- was quantificationally analyzed by the Griess method.[2] Firstly, the coloring reagent for NO_2^- was prepared as follow: 0.1 g of N-(1-naphthyl)-ethylenediamine dihydrochloride, 1.0 g of sulfonamide and 2.94 mL of H_3PO_4 were dissolved in 50 mL of deionized water. Next, 40 μL catholyte was diluted to 2 mL and 1 mL of diluted solution was mixed with 1 mL of coloring reagent and 2 mL of deionized water. After shaking and standing for 10 minutes, the UV-Vis spectrophotometry was used to measure the absorbance at a wavelength of 540 nm. The concentration of NO_2^- was calculated based on the calibration curve (y = 0.22227x + 0.02882, R^2 = 0.999).

Determination of N_2H_4: In this work, we used the method of Watt and Chrisp to estimate whether N_2H_4 produced.[3] The chromogenic reagent was a mixed solution of 5.99 g $C_9H_{11}NO$, 30 mL HCl and 300 mL C_2H_5OH. In detail, 1 mL electrolyte was added into 1 mL prepared coloring reagent and standing for 15 min in the dark. The absorbance at 455 nm was measured to quantify the N_2H_4 concentration with a standard curve of hydrazine (y = 0.67388x + 0.05274, R^2 = 0.9998).

Calculations of the FE and NH_3 yield rate:

FE toward NH_3 via NO_3RR was calculated by the following equation:

$$FE = (8 \times F \times [NH_3] \times V) / (M_{NH3} \times Q) \times 100\% \quad (1)$$

(Note that the reduction of NO_3^- to NH_3 consumes eight electrons.)

NH_3 yield rate is calculated using the following equation:

$$NH_3 \text{ yield rate} = ([NH_3] \times V) / (M_{NH3} \times t \times A) \quad (2)$$

Where F is the Faradaic constant (96500 C mol^{-1}), $[NH_3]$ is the measured NH_3 concentration, V is the volume of electrolyte in the cathode compartment (35 mL),

M_{NH3} is the molar mass of NH_3, Q is the total quantity of applied electricity; t is the electrolysis time and A is the loaded area of catalyst (0.5 × 0.5 cm^2).

DFT calculation details:

Density functional theory (DFT) is employed for all spin-polarized computations. The electron exchange and correlation are described by Perdew-Burke-Ernzerhof (PBE) functional within a generalized gradient approximation (GGA).[4,5] Projector augmented wave (PAW) method is employed to describe the electron-ion interaction. The kinetic energy cutoff for plane wave is set to be 400 eV. The Brillouin zone is sampled with a 3 × 3 × 1 k-points grid. Structures are optimized until the total energy and force of each atom reach the criteria of 10^{-4} eV and 0.02 eV/Å, respectively. vdWs effect in all computations was described by DFT-D3 method.[6] Different crystal facets were cleavaged to build the models for different facets. In a typical model, some bottom atoms were fixed and others were relaxed to model the surface. For example, in the model of Co (111) crystal facet, there were 27 atoms with fixed 9 bottom atoms. A 20 Å vacuum layer in z direction is introduced to avoid the interactions between adjacent Co crystal layers.

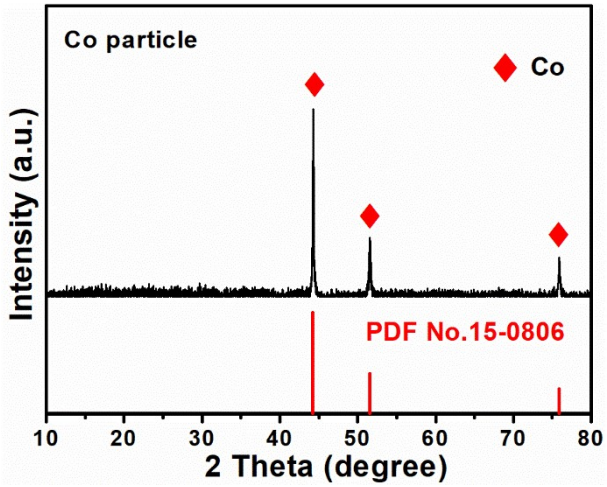

Fig. S1. XRD pattern for Co particle.

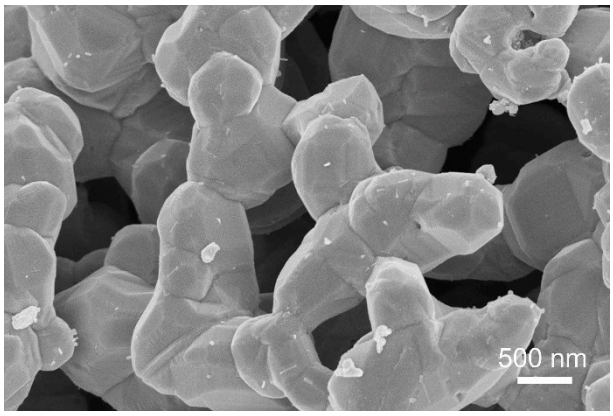

Fig. S2. SEM image for Co particle.

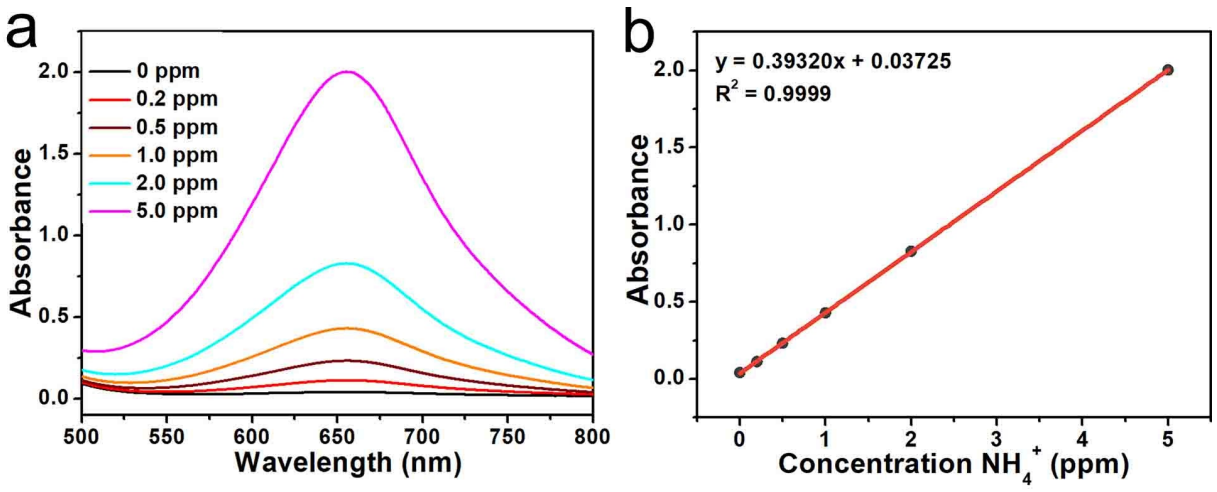

Fig. S3. (a) UV-Vis absorption spectra and (b) corresponding calibration curve used for calculation of NH_4^+ concentration.

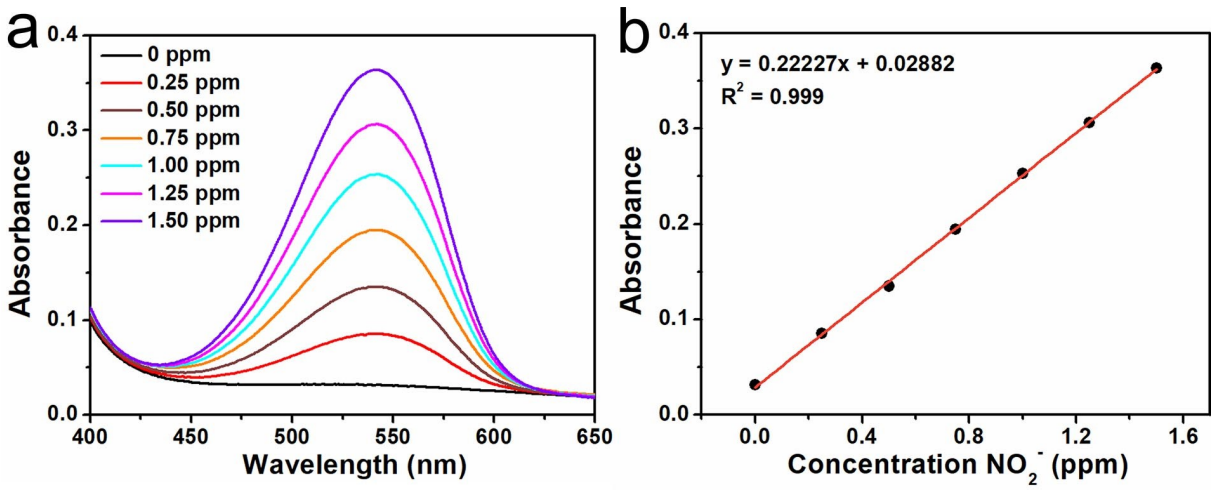

Fig. S4. (a) UV-Vis absorption spectra and (b) corresponding calibration curve used for calculation of NO_2^- concentration.

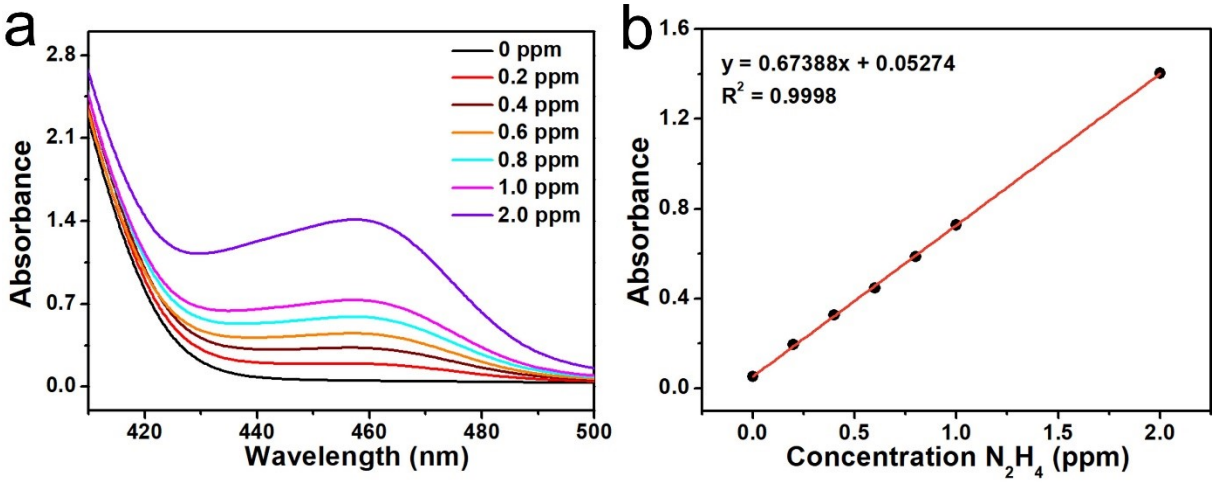

Fig. S5. (a) UV-Vis absorption spectra and (b) corresponding calibration curve used for calculation of N_2H_4 concentration.

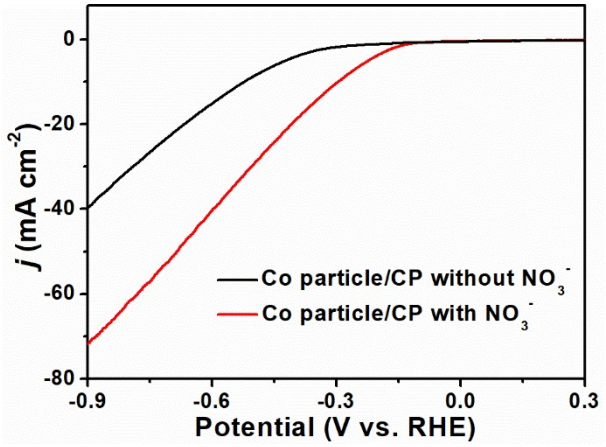

Fig. S6. LSV curves of Co particle/CP in 0.1 M NaOH with and without NO_3^-.

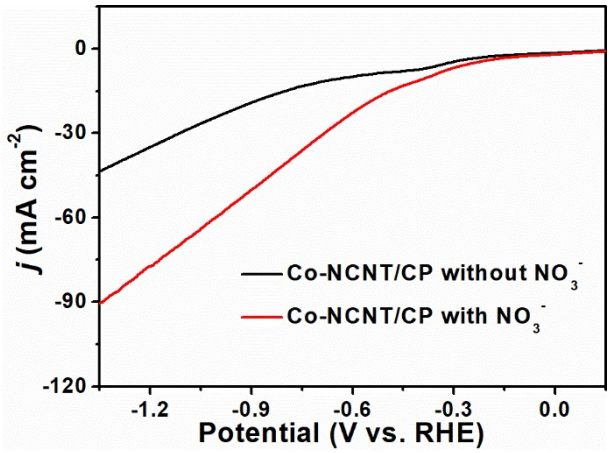

Fig. S7. LSV curves of Co-NCNT/CP in 0.1 M PBS with and without 0.1 M NO_3^-.

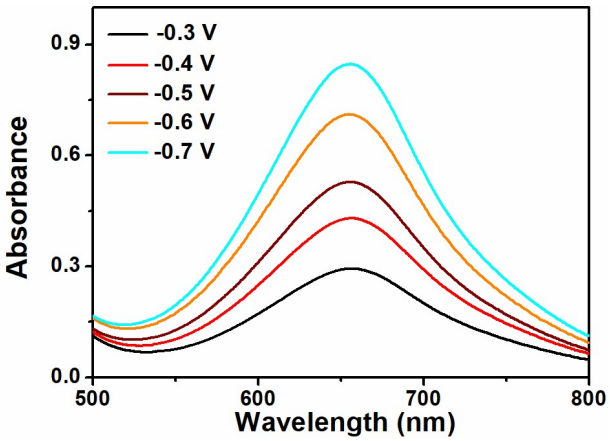

Fig. S8. UV-Vis absorption spectra of the colored electrolytes after 2-h electrolysis.

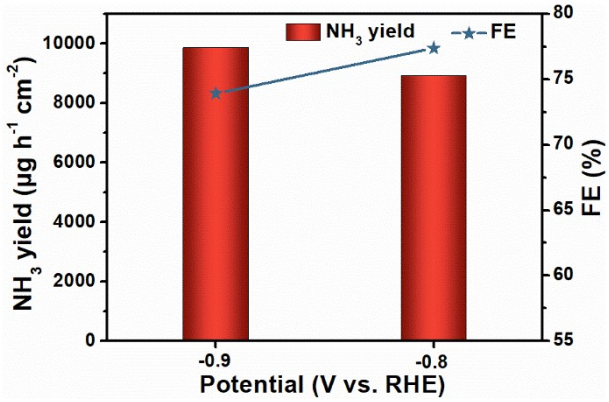

Fig. S9. NH_3 yields and FEs at –0.8 V and –0.9 V.

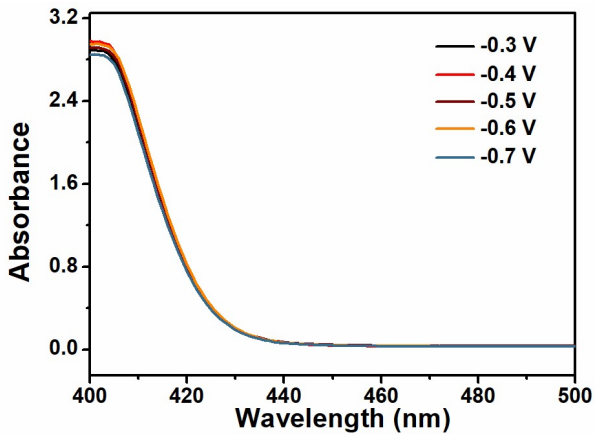

Fig. S10. UV-Vis absorption spectra of produced N_2H_4 for Co-NCNT/CP estimated by the method of Watt and Chrisp after 2-h electrolysis at each given potential.

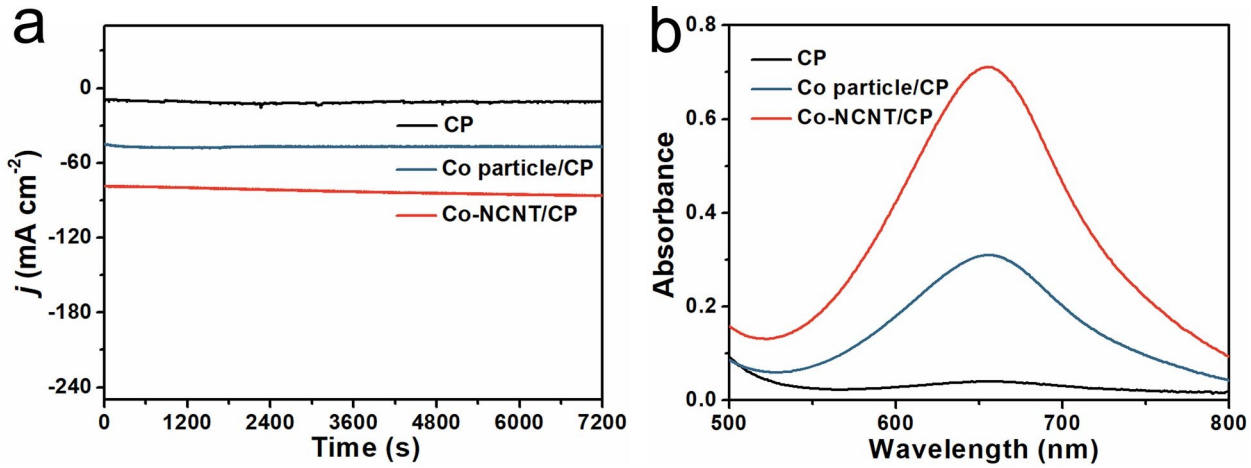

Fig. S11. (a) CA curves of bare CP, Co-NCNT/CP, and Co particle/CP for NO_3RR at –0.6 V in 0.1 M NaOH with 0.1 M NO_3^-. (b) Corresponding UV-Vis absorption spectra of the electrolytes stained with indophenol indicator after 2-h electrolysis.

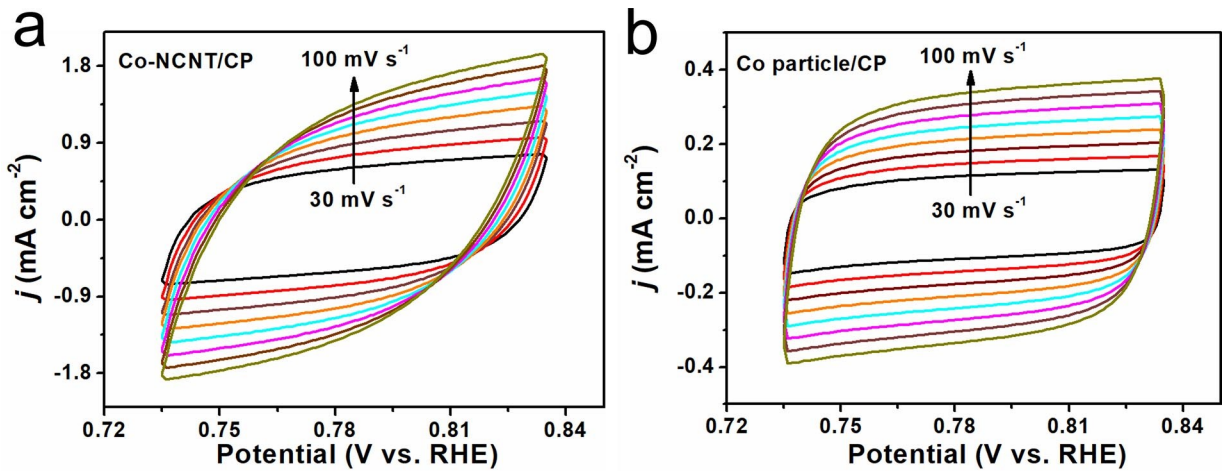

Fig. S12. CV curves of (a) Co-NCNT/CP and (b) Co particle/CP recorded in the non-Faradaic region of 0.735–0.835 V at various scan rates (30–100 mV s^{-1}). The electrochemical double-layer capacitances (C_{dl}) are the slopes of the linear fits.

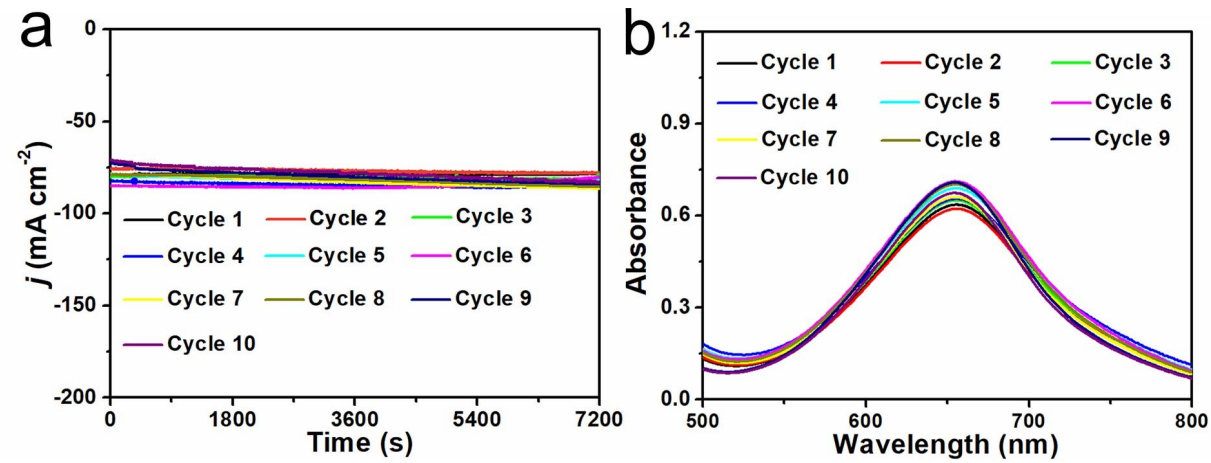

Fig. S13. (a) CA curves for Co-NCNT/CP during recycling tests toward NO_3RR at –0.6 V in 0.1 M NaOH with 0.1 M NO_3^-. (b) Corresponding UV-Vis absorption spectra of the electrolytes stained with indophenol indicator after recycling tests.

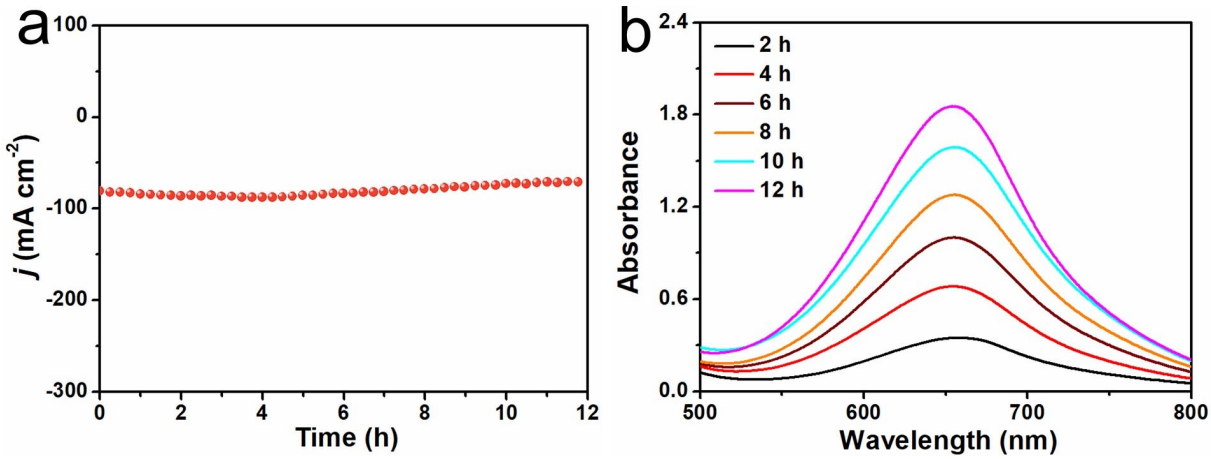

Fig. S14. (a) Long-term stability test of Co-NCNT/CP at −0.6 V in 0.1 M NaOH with 0.1 M NO_3^-. (b) Corresponding UV-Vis absorption spectra of the electrolytes stained with indophenol indicator after 12-h electrolysis.

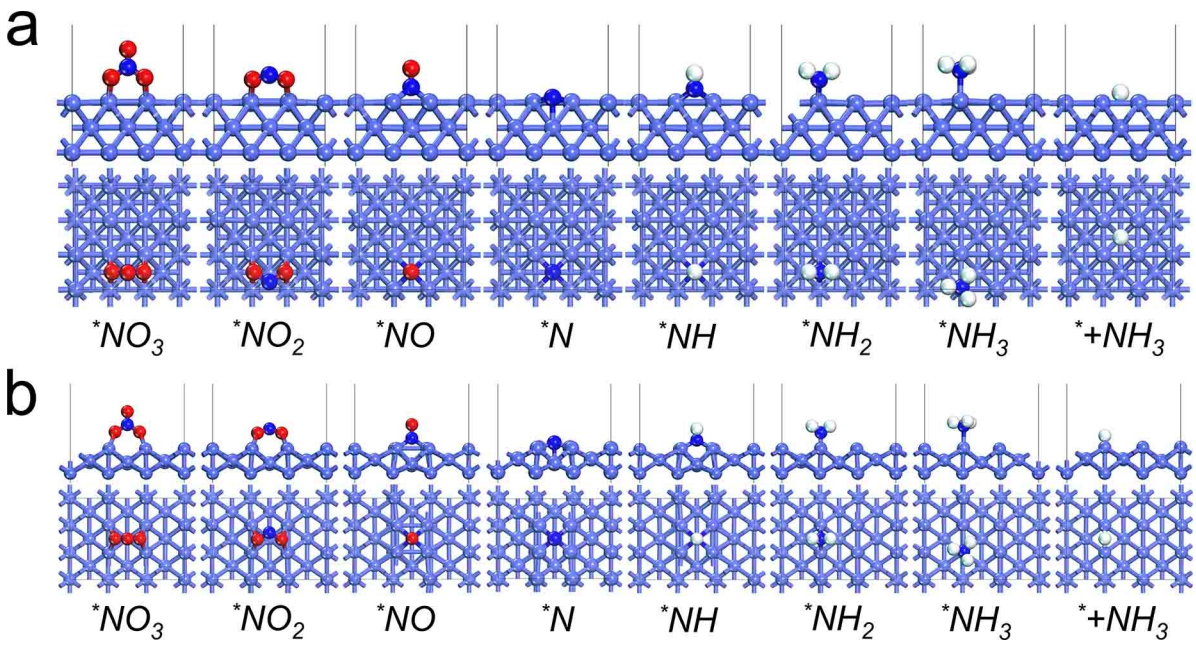

Fig. S15. Atomic configurations of NO_3RR intermediates on (a) Co (200) and (b) Co (220) surfaces from side and top view.

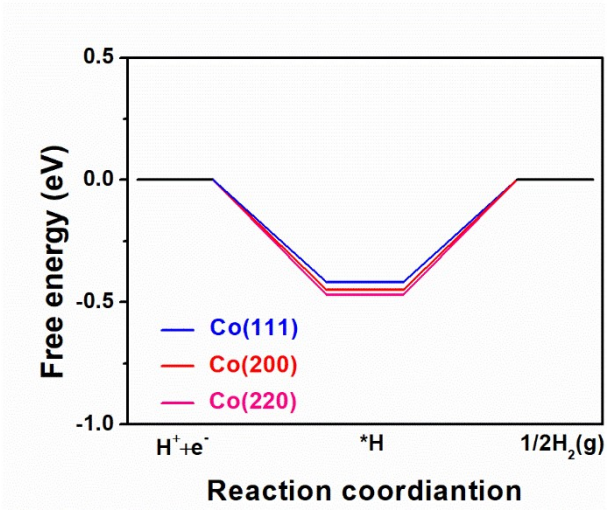

Fig. S16. Gibbs free energy profiles of HER on the Co (111), Co (200), and Co (220) planes. Energy barrier values of HER for Co (111), Co (200) and Co (220) are 0.41 eV, 0.45 eV, and 0.47 eV, respectively.

Table S1 Comparison of performance for Co-NCNT nanohybrid with other reported NO_3RR electrocatalysts.

Catalyst	Electrolyte	Potential (V vs. RHE)	NH_3 yield ($\mu g\ h^{-1}\ cm^{-2}$)	FE (%)	C_{dl} ($mF.cm^{-2}$)	Ref.
Co-NCNT	0.1 M NaOH (0.1 M NO_3^-)	−0.60	5996	92	12.13	This work
PTCDA/O-Cu	0.1 M PBS (500 ppm NO_3^-)	−0.40	435	77	/	7
$Cu_{50}Ni_{50}$	0.1 M KOH (0.1 M NO_3^-)	0	/	84.0	2.45	8
Co-P	0.2 M Na_2SO_4 (200 ppm NO_3^-)	−0.30	350	93.6	/	9
Pd/TiO_2	0.5 M NaOH (0.25 M NO_3^-)	−0.7	1120	92	5.51	10
Cu nanosheets	0.1 M KOH (10 mM NO_3^-)	−0.15	390.1	99.7	/	11
Fe-PPy SACs	0.1 M KOH (0.1 M NO_3^-)	−0.70	2749	~100	/	12
Pd Facets	0.1 M NaOH (20 mM NO_3^-)	−0.20	306.8	35	/	13
TiO_{2-x}	0.5 M Na_2SO_4 (50 ppm NO_3^-)	−0.94	765	85.0	/	14
$Ni(OH)_2$@Ni	100 mM Na_2SO_4 (200 mg L^{-1} NO_3^-)	/	/	64.4	0.263	15
Fe SAC	0.1 M K_2SO_4 (0.5 M NO_3^-)	−0.66	7820	75	2.06	16
Cu/Cu_2O NWAs	0.5 M Na_2SO_4 (200 ppm NO_3^-)	−0.85	4163.3	95.8	1	17
Cu	1 M NaOH (0.1 M NO_3^-)	/	/	79%	0.028	18
Co/CoO NSA	0.1 M Na_2SO_4 (200 ppm NO_3^-)	−0.65	3305.8	93.8	5.78	19

References

1 D. Zhu, L. Zhang, R. E. Ruther and R. J. Hamers, *Nat. Mater*., 2013, **12**, 836–841.

2 L. C. Green, D. A. Wagner, J. Glogowski, P. L. Skipper, J. S. Wishnok and S. R. Tannenbaum, *Anal. Biochem*., 1982, **126**, 131–138.

3 G. W. Watt and J. D. Chrisp, *Anal. Chem*., 1952, **24**, 2006–2008.

4 Y. Li, F. Gong, Q. Zhou, X. Feng, J. Fan and Q. Xiang, *Appl. Catal. B,* 2020, **268**, 118381.

5 F. Gong, Z. Ding, Y. Fang, C. Tong, D. Xia, Y. Lv, B. Wang, D. V. Papavassiliou, J. Liao and M. Wu, *ACS Appl. Mater. Interfaces,* 2018, **10**, 14614–14621.

6 F. Gong, H. Li, Q. Zhou, M. Wang, W. Wang, Y. Lv, R. Xiao and D. V. Papavassiliou, *Nano Energy,* 2020, **74**, 104922.

7 G. Chen, Y. Yuan, H. Jiang, S. Ren, L. Ding, L. Ma, T. Wu, J. Lu and H. Wang, *Nat. Energy,* 2020, **5**, 605–613.

8 Y. Wang, A. Xu, Z. Wang, L. Huang, J. Li, F. Li, J. Wicks, M. Luo, D. Nam, C. Tan, Y. Ding, J. Wu, Y. Lum, C. Dinh, D. Sinton, G. Zheng and E. H. Sargent, *J. Am. Chem. Soc.,* 2020, **142**, 5702–5708.

9 Z. Li, G. Wen, J. Liang, T. Li, Y. Luo, Q. Kong, X. Shi, A. M. Asiri, Q. Liu and X. Sun, *Chem. Commun.,* 2021, **57**, 9720–9723.

10 Y. Guo, R. Zhang, S. Zhang, Y. Zhao, Q. Yang, Z. Huang, B. Dong and C. Zhi, *Energy Environ. Sci.,* 2021, **14**, 3938–3944.

11 X. Fu, X. Zhao, X. Hu, K. He, Y. Yu, T. Li, Q. Tu, X. Qian, Q. Yue, M. R. Wasielewski and Y. Kang, *Appl. Mater. Today,* 2020, **19**, 100620.

12 P. Li, Z. Jin, Z. Fang and G. Yu, *Energy Environ. Sci.,* 2021, **14**, 3522–3531.

13 J. Lim, C. Liu, J. Park, Y. Liu, T. P. Senftle, S. W. Lee and M. C. Hatzell, *ACS Catal.,* 2021, **11**, 7568–7577.

14 R. Jia, Y. Wang, C. Wang, Y. Ling, Y. Yu and B. Zhang, *ACS Catal.,* 2020, **10**, 3533–3540.

15 W. Zheng, L. Zhu, Z. Yan, Z. Lin, Z. Lei, Y. Zhang, H. Xu, Z. Dang, C. Wei and C. Feng, *Environ. Sci. Technol.,* 2021, **55**, 13231–13243.

16 Z. Wu, M. Karamad, X. Yong, Q. Huang, D. A. Cullen, P. Zhu, C. Xia, Q. Xiao, M. Shakouri, F. Chen, J. Y. Kim, Y. Xia, K. Heck, Y. Hu, M. S. Wong, Q. Li, I. Gates, S. Siahrostami and H. Wang, *Nat. Commun.,* 2021, **12**, 2870.

17 Y. Wang, W. Zhou, R. Jia, Y. Yu and B. Zhang, *Angew. Chem., Int. Ed.,* 2020, **59**, 5350–5354.

18 D. Reyter, G. Chamoulaud, D. Bélanger and L. Roué, *J. Electroanal. Chem.,* 2006, **596**, 13–24.

19 Y. Yu, C. Wang, Y. Yu, Y. Wang and B. Zhang, *Sci. China Chem.,* 2020, **63**, 1469–1476.